THE JOURNAL OF PHYSICAL CHEMISTRY B
A JOURNAL OF THE AMERICAN CHEMICAL SOCIETY

pubs.acs.org/JPCB

Perspective

Pair-Reaction Dynamics in Water: Competition of Memory, Potential Shape, and Inertial Effects

Florian N. Brünig, Jan O. Daldrop, and Roland R. Netz*

Cite This: *J. Phys. Chem. B* 2022, 126, 10295−10304

Read Online

ACCESS | Metrics & More | Article Recommendations | Supporting Information

ABSTRACT: When described by a one-dimensional reaction coordinate, pair-reaction rates in a solvent depend, in addition to the potential barrier height and the friction coefficient, on the potential shape, the effective mass, and the friction relaxation spectrum, but a rate theory that accurately accounts for all of these effects does not exist. After a review of classical reaction-rate theories, we show how to extract all parameters of the generalized Langevin equation (GLE) and, in particular, the friction memory function from molecular dynamics (MD) simulations of two prototypical pair reactions in water, the dissociation of NaCl and of two methane molecules. The memory exhibits multiple time scales and, for NaCl, pronounced oscillatory components. Simulations of the GLE by Markovian embedding techniques accurately reproduce the pair-reaction kinetics from MD simulations without any fitting parameters, which confirms the accuracy of the approximative form of the GLE and of the parameter extraction techniques. By modification of the GLE parameters, we investigate the relative importance of memory, mass, and potential shape effects. Neglect of memory slows down NaCl and methane dissociation by roughly a factor of 2; neglect of mass accelerates reactions by a similar factor, and the harmonic approximation of the potential shape gives rise to slight acceleration. This partial error cancellation explains why Kramers' theory, which neglects memory effects and treats the potential shape in harmonic approximation, describes reaction rates better than more sophisticated theories. In essence, all three effects, friction memory, inertia, and the potential shape nonharmonicity, are important to quantitatively describe pair-reaction kinetics in water.

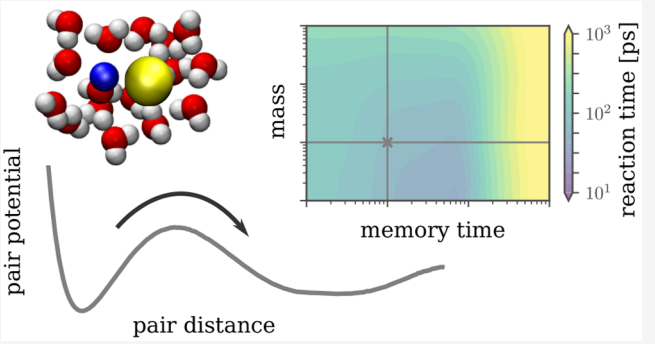

INTRODUCTION

Pair reactions in water, such as the association and dissociation of ions or hydrophobic molecules, are fundamental in biological and chemical processes and are commonly described by diffusive motion of the pair distance in a one-dimensional potential landscape.[1−4] The most important signatures of such reactions are the rates at which a pair dissociates or is created, which determine the turnover of complex biological reaction networks and the efficiency of large-scale chemical applications. Reaction-rate theory has a long history and dates back to Arrhenius,[5] who discovered the exponential dependence of reaction time on the free-energy or potential barrier height that separates reactants and products along a suitably chosen reaction coordinate. In a solvent, the reacting solutes experience friction,[1−4,6−8] which determines the pre-exponential factor of the Arrhenius law. But the mass of the reactants also influences the rate of a reaction. In fact, in his landmark paper, Kramers showed that reaction times exhibit a minimum at an intermediate value of the ratio of the effective friction and mass of a given reaction coordinate, a phenomenon that is called Kramers' turnover.[1,9]

However, the assumption of instantaneous friction, employed in early theories, breaks down whenever there is no pronounced separation between time scales of fast solvent relaxation and slow diffusion along the reaction coordinate, which is the case even for the simplest pair reactions in water.[10,11] One strategy is to circumvent such non-Markovian effects and to reduce friction memory by using suitable multidimensional reaction coordinates that explicitly account for solvent degrees of freedom.[12−15] Alternatively, the generalized Langevin equation (GLE),[16,17] which explicitly accounts for time-dependent friction due to solvent relaxation, can be used to model reaction rates[18−34] and transition-path times.[35−37]

Different analytical rate theories based on the GLE have been developed but necessarily rely on various approximations, the effects of which are difficult to disentangle.[22,32,38,39] This is where numerical solutions of accurately parametrized GLEs

Received: August 18, 2022
Revised: November 11, 2022
Published: December 6, 2022

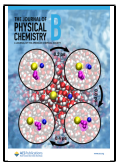

become instrumental. The extraction of memory kernels from general time series data is an active field of research,[33,40−45] in particular in the context of reaction kinetics.[10,30,46−49] With recent methodological advances, it is possible to extract memory kernels from trajectories in the presence of arbitrary, not necessarily harmonic, potentials and to numerically solve the resulting GLE by Markovian embedding techniques.[23,31,50,51] While the one-dimensional GLE may in principle contain nonlinear friction contributions, the approximate linear friction GLE, which only includes a linear coupling of the velocity to a friction kernel with no further dependencies on position or velocity, becomes valid for a broad class of systems under well-defined conditions;[52] this explains why it accurately describes the dynamics of very different physical systems.[31,51] In this connection, it is important to note that most existing reaction-rate theories are in fact based on the approximate linear friction GLE.

As simple model systems, we consider the dissociation and association kinetics of two different pair reactions in water, NaCl and methane, which exhibit drastically different hydration properties. Ions are favorably dissolved in water by the formation of a strongly ordered hydration shell,[53−55] whereas nonpolar small objects such as methane are repelled from water and induce strong water−water hydrogen bonding in their hydration shell.[56−58] In fact, NaCl ion-pair dissociation in water has been widely studied,[12−14,30,46,49,54,59−64] and the failure of a Markovian kinetic model along a one-dimensional reaction coordinate,[12,13,62,65] the relevance of inertial[62] and memory effects,[30,46,49,61] has been demonstrated. In contrast, the reaction dynamics of hydrophobic molecules has received less attention. We analyze the reaction dynamics of these two systems based on extensive MD simulation trajectories of single reactant pairs in explicit water, from which we extract all parameters of the one-dimensional linear friction GLE in terms of the natural reaction coordinate, namely, the distance between the two reactants: These are the potential (or free-energy) landscape, the reduced mass, and the memory friction kernel that in general exhibits multiple time scales and oscillatory components.

As a crucial first step, we demonstrate by simulations of the GLE that it accurately reproduces the kinetics of the underlying MD simulations, which is nontrivial since the GLE could in principle also contain nonlinear friction contributions.[52,66] In a second step, we investigate how the pair-dissociation kinetics change when we independently vary the memory times and the effective mass, encompassing the Markovian limit of vanishing memory time and the overdamped limit of vanishing mass.

Throughout this paper, we determine reaction rates from mean first-passage times, τ_{MFP}, which can be conveniently extracted from long simulation trajectories and which accurately reproduce barrier escape times, as we have shown previously.[22] We find that for both NaCl and methane, the neglect of memory slows down dissociation by roughly a factor of 2, while the neglect of mass accelerates dissociation by a similar factor. When neglecting both memory and mass, partial error cancellation takes place, but dissociation still slows down considerably. Approximating the free-energy landscape by a harmonic barrier also introduces significant errors. Thus, it transpires that for the quantitative prediction of reaction times, memory, finite mass, and nonharmonic potential effects must be simultaneously taken into account, and the GLE is the appropriate tool to disentangle the effects of these different contributions on reaction times.

The free-energy barriers for the dissociation of NaCl and methane are about 4 k_BT and 2 k_BT, respectively; these are typical barrier heights not only of molecular association and dissociation reactions in water but also of dihedral stereoisomerization[23] as well as fast protein folding transitions.[67] Most reaction-rate theories rest on assumptions that become only valid in the limit of high free-energy barriers. Since many transitions in biophysical chemistry are in fact characterized by rather low barrier heights of the order of only a few k_BT and experimental transition rates are customarily interpreted in terms of reaction-rate theories, we therefore also compare the results from our simulations with reaction-rate-theory predictions. Interestingly, it turns out that, due to partial error compensation, Kramers' theory,[1] which neglects memory as well as nonharmonic potential effects, predicts the NaCl dissociation time better than Grote/Hynes (GH) theory,[38] which only neglects nonharmonic potential effects. It follows that agreement between the predictions of a particular reaction-rate theory and experimental or simulation results does not necessarily mean that the approximations made in deriving the reaction-rate theory are valid for the specific system.

SIMULATION MODEL AND THEORETICAL FRAMEWORK

We analyze the dynamics of single NaCl and methane pairs from MD simulations in SPC/E water at 300 K as described in the Methods section. The distance between the two reactants is used as the reaction coordinate x, along which a weak harmonic confining potential $U_{con}(x) = kx^2/2$ is applied to prevent the reactants from diffusing apart and thereby to increase the number of association and dissociation events. The potential or free energy of a NaCl ion pair, $U(x) = -k_BT\log(p(x))$, obtained from the distribution function $p(x)$, is shown in Figure 1A as a solid line. The contact pair (CP) state is separated by a barrier of 4.37 k_BT, located at the transition state (TS), from the solvent-separated pair (SSP) state. Snapshots from the MD simulation illustrate the different states in Figure 1A. In fact, the TS in this one-dimensional projection corresponds to an ensemble of disparate states that do not single out well the actual TS in an enlarged multidimensional description.[12,15] This however is not a problem for our kinetic description using the GLE, since non-Markovian effects, caused by dimensional reduction, are fully accounted for. Note that the confinement potential $U_{con}(x)$ changes the barrier height from the CP to the TS state slightly, as seen by comparing $U(x)$ (solid line) and $U(x) - U_{con}(x)$ (broken line) in Figure 1A. Thus, the presence of a confining potential influences the reaction times, and it in fact also influences the shape of the extracted memory kernel, in agreement with previous results for confined molecules[68] (see Supporting Information (SI) section I for details); this, however, does not affect our general conclusions that memory, inertial, and potential-shape effects influence barrier-crossing times. The actual NaCl interaction potential, obtained by subtracting the centrifugal contribution and the confinement potential, $U_{int}(x) = U(x) - U_{con}(x) + 2k_BT\log(x)$ (dotted line in Figure 1A), goes for large separations x to a constant. Note that in order to describe the simulated NaCl pair dynamics along x, the potential $U(x)$ has to be used within the GLE.

https://doi.org/10.1021/acs.jpcb.2c05923
J. Phys. Chem. B 2022, 126, 10295−10304

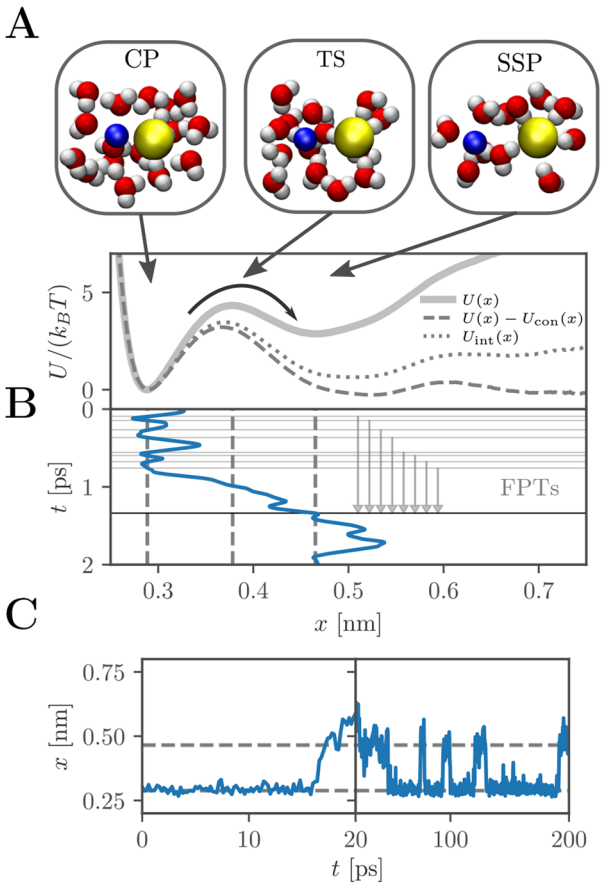

Figure 1. (A) Effective potential $U(x)$ of a single NaCl ion pair in SPC/E water as a function of the ion separation x as obtained from molecular dynamics (MD) simulations in the presence of a weak harmonic confining potential $U_{con}(x)$ (solid line). The broken line denotes $U(x) - U_{con}(x)$, and the dotted line denotes the interaction potential $U_{int}(x)$ for which also the centrifugal potential contribution has been subtracted. Snapshots from the MD simulations illustrate the contact pair (CP), the solvent-separated pair (SSP) (both at the potential minima), and the transition state (TS) at the potential maximum. (B,C) Example trajectories of the interionic distance x on three different time scales, 2, 20, and 200 ps. The mean first-passage time τ_{MFP} between the initial CP state and the final SSP state is calculated from the average of all first-passage times (FPTs); see main text for details.

In the following, we concentrate on the dissociation kinetics starting from the CP state, which we characterize by the mean first-passage time, τ_{MFP}.[22] For this, we obtain from a single long MD trajectory first-passage times (FPTs), defined as the time span between passing through the initial position x_i and reaching the final position x_f for the first time. In Figure 1B, a few FPTs for the passage from the CP to the SSP state from an actual MD trajectory are shown, the average of all FPTs gives τ_{MFP}. In Figures 1B,C, the dynamics of the NaCl ion-pair separation is shown on three different time scales, which illustrates the stochastic nature of the barrier-crossing dynamics that is characterized by the waiting time in the CP state on the order of $\tau_{MFP} \approx 70$ ps.

In order to reveal the mechanisms that control the pair-reaction dynamics, we use the GLE that includes a general nonlinear potential $U(x)$ and a memory friction kernel $\Gamma(t)$:

$$m\ddot{x}(t) = -\int_0^t \Gamma(t-t')\dot{x}(t')\mathrm{d}t' - \nabla U[x(t)] + \eta(t) \quad (1)$$

Here, m is the effective mass and $\eta(t)$ is a Gaussian random force with vanishing mean $\langle\eta(t)\rangle = 0$ and correlations $\langle\eta(t)\eta(t')\rangle = k_BT\Gamma(t-t')$. The GLE in eq 1 neglects nonlinear friction effects, which is valid when correlations between velocities and random forces are independent of x[52] and has been successfully used to model the dynamics of protein folding and molecular vibrations.[31,51] We will further below validate the linear friction GLE in eq 1 by comparison with MD data. All parameters in eq 1 are extracted from simulation trajectories: The mass is obtained from the equipartition theorem $m = k_BT/\langle\dot{x}^2(t)\rangle$ and is demonstrated to be independent of x in SI section II, as indeed expected for a linear distance coordinate.[52] The potential follows from the distribution $p(x)$ via $U(x) = -k_BT\log(p(x))$, and the memory friction kernel $\Gamma(t)$ is extracted from the simulation trajectory by numerical inversion of eq 1.[31,51]

In order to validate the linear friction GLE and its parametrization, we need to compare predictions of the GLE with the MD simulation results. For this, the GLE is numerically solved using Markovian embedding, for which the memory kernel is parametrized as a sum of exponentially decaying and oscillating components according to[51,69−71]

$$\Gamma(t) = \sum_{i=0}^{n} \frac{\gamma_i^e}{\tau_i^e} \mathrm{e}^{-t/\tau_i^e} + \sum_{i=0}^{l} \frac{\gamma_i^o \mathrm{e}^{-t/\tau_i^o}}{2\tau_i^o(1+(\omega_i\tau_i^o)^2)^{-1}} \left[\cos(\omega_i t) + \frac{\sin(\omega_i t)}{\tau_i^o\omega_i}\right] \quad (2)$$

where τ_i^e and τ_i^o denote the memory times of the non-oscillating and oscillating memory components, ω_i denotes the oscillation frequency, and γ_i^e and γ_i^o denote the amplitudes of the memory components. The parametrization of the memory kernel is done in a way such that the long-time friction coefficient γ, defined by the integral $\gamma = \int_0^\infty \Gamma(t)\mathrm{d}t$, is given by $\gamma = \sum_i \gamma_i^e + \sum_i \gamma_i^o$ and thus is independent of the memory time scales.

In the Markovian limit, i.e., when all memory times go to zero, the memory kernel takes the form $\Gamma(t) \to 2\gamma\delta(t)$. In this limit, the GLE eq 1 reduces to the ordinary Langevin equation (LE)[72]

$$m\ddot{x}(t) = -\gamma\dot{x}(t) - \nabla U[x(t)] + \xi(t) \quad (3)$$

where the random force $\xi(t)$ has zero mean and is correlated according to $\langle\xi(t)\xi(t')\rangle = 2\gamma k_BT\delta(t-t')$. In the limit $m \to 0$, the overdamped LE is obtained from eq 3, which neglects memory as well as inertial effects. The numerical effort of simulating the GLE in eq 1 is linear in the number of fit functions in eq 2 and thus amounts to $n + l + 1$ times the effort of simulating the LE in eq 3. Additionally, the simulation effort scales as the inverse of the discretization time step, which has to be on the order of the shortest time scale of the system, which can be either the shortest memory time scale in eq 2 or the inertial time scale m/γ.

Most analytical rate theories are on the harmonic level and approximate the potential quadratically around the barrier top and the potential well. We investigate the accuracy of this approximation, which becomes exact only in the infinite-barrier height limit, in SI section III by a perturbation analysis in terms

https://doi.org/10.1021/acs.jpcb.2c05923
J. Phys. Chem. B 2022, 126, 10295−10304

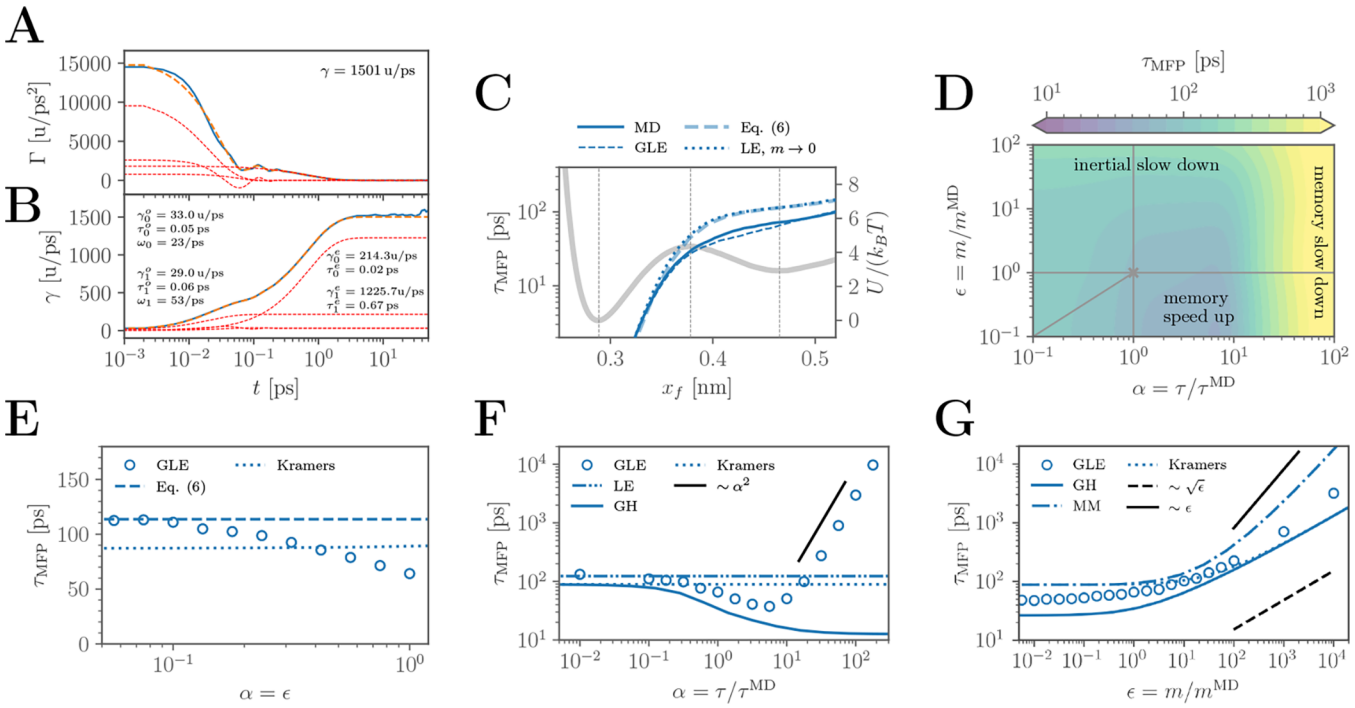

Figure 2. Analysis of NaCl dissociation dynamics in water. (A,B) Memory friction kernel (A) and its integral (B) from MD simulations (blue solid lines) compared with a fit according to eq 2 (yellow broken lines) which is a sum of two exponential and two oscillatory components (red broken lines). The fit parameters are given in the legend. (C) Potential $U(x)$ is shown as a gray solid line (right scale) with the extrema indicated by vertical gray dotted lines. Profiles of $\tau_{MFP}(x_f)$ (left scale) starting from the CP state are shown from MD simulations (blue solid line), from simulations of the GLE eq 1 (blue short-dashed line), from the theory in the overdamped Markovian limit eq 6 (blue long-dashed line), and from simulations of the LE eq 3 in the zero-mass limit (blue dotted line). (D) Contour plot of the CP-SSP dissociation τ_{MFP} from GLE simulations as a function of the mass and memory-time scaling parameters ϵ and α. The gray solid lines illustrate the paths shown in (E−G). (E−G) τ_{MFP} for the CP-SSP dissociation reaction as a function of $\epsilon = \alpha$ (E), α for $\epsilon = 1$ (F), and ϵ for $\alpha = 1$ (G). Predictions according to Kramers' theory eq 4 (dotted lines), GH theory eq 5 (solid lines), MM theory (dashed-dotted line), and the overdamped Markovian theory eq 6 (broken lines) are shown for comparison. Simulations of the LE according to eq 3 are shown as a dash-double-dotted line in F. The error bars of the GLE simulation results in E−G are smaller than the symbol size.

of cubic and quartic potential corrections. The classical Kramers' expression for the escape of a massive particle over a barrier that is subject to memoryless friction, as described by LE eq 3, valid in the medium-to-high friction regime, reads[1]

$$\tau_{Kr} = \left[\left(\frac{\gamma^2}{4m^2} + \omega_{max}^2\right)^{1/2} - \frac{\gamma}{2m}\right]^{-1} \omega_{max}\tau_{TST} \tag{4}$$

where the barrier frequency $\omega_{max} = \sqrt{-U''_{max}/m}$ depends on the potential curvature $U''_{max} = U''(x_{max})$ at the barrier top located at x_{max}. For low friction $\gamma/m \to 0$, this expression reproduces the transition-state theory limit $\tau_{Kr} \to \tau_{TST} = 2\pi\omega_{min}^{-1}e^{\beta U_0}$, where $\beta^{-1} = k_BT$ is the thermal energy, U_0 denotes the barrier height, and $\omega_{min} = \sqrt{U''_{min}/m}$ is the oscillation frequency at the minimum x_{min} with $U''_{min} = U''(x_{min})$.[73] In the high-friction limit, $\gamma/m \to \infty$, eq 4 reduces to $\tau_{Kr} \to \frac{\gamma}{m\omega_{max}}\tau_{TST} = 2\pi\gamma e^{\beta U_0}/\sqrt{-U''_{max}U''_{min}}$ which is linear in the friction coefficient γ. Note that eq 4 misses the correct scaling in the low-friction or high-mass limit, $\tau_{MFP} \sim \frac{m}{\gamma\beta U_0}e^{\beta U_0}$, where τ_{MFP} scales inversely proportional to γ, which was also derived by Kramers.[1] An exact expression for τ_{MFP} in the Markovian limit, valid for arbitrary mass and friction and using the quadratic potential approximation, was derived by Mel'nikov and Meshkov (MM)[74] (see SI section IV).

The GH prediction for τ_{MFP} in the presence of memory acting at a harmonic barrier reads[38]

$$\tau_{GH} = \frac{\omega_{max}}{\lambda}\tau_{TST} \tag{5}$$

where the frequency λ is determined by the solution of the equation $\lambda = \omega_{max}^2/(\lambda + \tilde{\Gamma}(\lambda)/m)$ and $\tilde{\Gamma}(\lambda)$ denotes the Laplace-transformed memory friction kernel $\Gamma(t)$ acting at the barrier. In the Markovian limit, i.e., for short memory time, one has $\tilde{\Gamma}(\lambda) = \gamma$ and the GH expression reduces to the Kramers' medium-to-high-friction result in eq 4. Note that in the limit of high mass or long memory time, GH theory reproduces the transition-state theory result, $\tau_{GH} = \tau_{TST}$, which means that it misses both the correct high-mass limit, characterized by $\tau_{MFP} \sim \frac{m}{\gamma\beta U_0}e^{\beta U_0}$,[1,74] as well as the correct long-memory-time limit, where τ_{MFP} scales as $\tau_{MFP} \sim \tau^2 e^{\beta U_0}$.[22,39]

In the overdamped Markovian limit, nonharmonic potential effects can be analytically treated and τ_{MFP} between initial and final positions, x_i and x_f, is given as[75]

$$\tau_{MFP}(x_i, x_f) = \beta \int_{x_i}^{x_f} dx'\gamma(x')e^{\beta U(x')} \int_{x_{min}}^{x'} dx e^{-\beta U(x)} \tag{6}$$

https://doi.org/10.1021/acs.jpcb.2c05923
J. Phys. Chem. B 2022, 126, 10295−10304

Here, $\gamma(x)$ denotes a general position-dependent friction profile and x_{min} a reflecting boundary. Equation 6 can be inverted and thereby used to determine $\gamma(x)$ from measured profiles of $\tau_{MFP}(x_i, x_f)$.[76,77] In fact, position-dependent friction, determined by a different approach, has been shown to reproduce NaCl dissociation dynamics from simulations.[63] However, memory effects give rise to spurious spatially dependent friction profiles when analyzed on the Markovian level.[31] Furthermore, spatially dependent friction cannot simultaneously describe dissociation and association kinetics, which demonstrates the presence and importance of memory, as shown in SI section V. In fact, the assumption of a friction memory kernel that is independent of position is in this paper shown to be very accurate; the Markovian assumption, i.e., the neglect of memory effects, on the contrary is shown not to be accurate. As we demonstrate in SI section III, using a harmonic approximation for the free energy $U(x)$ around its minimum and its barrier and in the high-barrier limit, the τ_{MFP} between arbitrary initial and final positions to the left and right of a barrier predicted by eq 6 equals the Kramers' prediction eq 4 in the high-friction limit. In fact, the Kramers', MM, and GH rate theories do not depend on the precise locations of the initial and final positions of τ_{MFP}, which is a consequence of the high-barrier assumption inherent in their derivations, but the dependence of τ_{MFP} on the final position is not very pronounced (the dependence of τ_{MFP} on the initial position is even weaker and displayed in SI section VI). It therefore is instructive to compare analytical rate-theory results for τ_{MFP} with MD and GLE simulation results. We show in SI section III by a perturbative analysis beyond the harmonic approximation that deviations between the Kramers' high-friction approximation and eq 6 are for not too low barrier height mostly due to the harmonic approximation and not so much due to the high-barrier assumption, which opens up routes to systematically improve upon literature rate theories.

RESULTS AND DISCUSSION

The memory kernel $\Gamma(t)$ for NaCl extracted from MD simulations is shown in Figure 2A (blue line), and its running integral in Figure 2B (blue line) starts to increase at a few fs and plateaus at about 4 ps. The shape of $\Gamma(t)$ is rather similar to previous results for single anions and cations in water,[78] which demonstrates that memory is caused not only by ion−ion interactions but also by hydration effects. A fit using the sum of two exponentially decaying and two oscillating components according to eq 2, shown in Figure 2A,B as a yellow broken line, is in near perfect agreement with the extracted data and will be used for all further GLE modeling. The individual memory components are shown as red broken lines, and their parameters are given in the legend.

In Figure 2C, the potential $U(x)$ is shown (gray line) together with the $\tau_{MFP}(x_f)$ profile from MD (blue solid line) for an initial position x_i at the minimum of $U(x)$ as a function of the final positions x_f, which corresponds to dissociation from the CP state (corresponding results for the inverse association reaction are reported in SI section VII). The dependence of τ_{MFP} on the initial position x_i is very weak, as demonstrated and analytically explained in SI section VI. The $\tau_{MFP}(x_f)$ profile from the GLE eq 1 with all parameters extracted from MD simulations (blue short-dashed line) agrees very well with the MD data (blue solid line). This presents a crucial validation of the linear friction GLE eq 1 and of the extracted parameters.

The GLE is not only able to reproduce the MD data, it also allows us to analyze the effects of varying mass and memory times on the dissociation kinetics in a nonharmonic potential landscape, which is not possible with MD simulations and also not with analytical rate theories. For this, we scale the mass m in the GLE by a factor ϵ according to $m = \epsilon m^{MD}$. Likewise, we scale all memory times by a second factor α according to $\tau_i = \alpha\tau_i^{MD}$ and $\omega_i = \alpha^{-1}\omega_i^{MD}$, which ensures a smooth crossover to the Markovian limit as $\alpha \to 0$. Since the friction coefficient γ is independent of α, by changing the value of α we are able to disentangle the effects of memory times and memory amplitudes, the latter being characterized by the friction coefficient γ, on the reaction kinetics. In the overdamped Markovian limit, i.e. for $\alpha, \epsilon \to 0$, τ_{MFP} is given by eq 6, shown as a long-dashed line in Figure 2C and compared with simulations of the LE eq 3 in the $m \to 0$ limit (dotted line). Both results agree nicely with each other, validating the numerical procedures used, but exhibit significantly longer τ_{MFP} than the MD data by a factor of almost two to the right of the free-energy barrier, which clearly demonstrates the significance of inertia and memory effects for reaction dynamics.

The effect of gradually and simultaneously reducing inertial and memory effects is demonstrated in Figure 2E, where τ_{MFP} from the CP to the SSP state obtained using the GLE is shown as a function of $\alpha = \epsilon$ (circles). The overdamped Markovian limit from eq 6 (broken horizontal line) is approached by the GLE data in the limit $\alpha = \epsilon \to 0$, as expected. The Kramers' prediction eq 4 (dotted line) is evaluated using the friction coefficient γ and mass m extracted from the MD data and using the fitted potential curvatures U''_{min} and U''_{max} in the well and at the barrier top (see SI section VIII for details of the fitting procedure). It exhibits an almost negligible dependence on ϵ, which shows that in the Markovian limit there are no discernible inertial effects. The significant difference between the broken and dotted lines is due to the harmonic-potential and high-barrier approximation in Kramers' theory. Interestingly, the Kramers' prediction (dotted line) is for $\alpha = \epsilon = 1$ closer to the GLE result than the more accurate numerical solution of eq 6 (broken horizontal line) which does not use the harmonic-potential nor the high-barrier approximation; this is due to a subtle error compensation between the harmonic-potential/high-barrier and Markovian approximations, as we will discuss in more detail further below. As mentioned before, due to the high-barrier approximation, the Kramers' prediction does not depend on the locations of the initial and final positions used in the definition of τ_{MFP} (as is the case for the MM and GH reaction-rate theories), while the MD and GLE simulation results obviously do, as demonstrated in Figure 2C and in SI Section VI. This is a general shortcoming of the high-barrier approximation employed in analytical theories and should be kept in mind when comparing with MD or GLE simulation results.

To disentangle inertial and memory effects, we in Figure 2F show τ_{MFP} for NaCl dissociation from the CP to the SSP state using the GLE eq 1 as a function of the memory scaling parameter α for original mass $\epsilon = 1$ (circles). τ_{MFP} exhibits a pronounced minimum close to the original memory time $\alpha = 1$, which demonstrates that memory accelerates barrier crossing for short and intermediate memory times but slows down barrier crossing for very long memory times. The barrier-crossing speed up for intermediate memory times, including

https://doi.org/10.1021/acs.jpcb.2c05923
J. Phys. Chem. B 2022, 126, 10295−10304

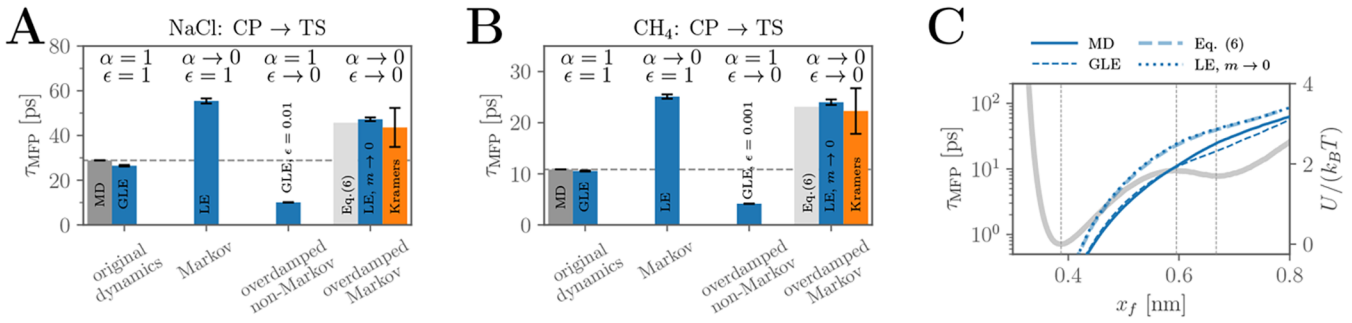

Figure 3. (A,B) Summary of memory friction and mass effects on the pair dissociation dynamics of NaCl and methane in water at 300 K. The bars denote τ_{MFP} from the CP to the TS state from MD (gray bars and horizontal broken lines) and from simulations of the GLE eq 1 (blue bars) in the different limits of the memory and mass scaling parameters, α and ϵ. The theoretical overdamped Markovian limit eq 6 is shown as light-gray bars, and Kramers' theory eq 4 for high friction is shown as yellow bars. Error bars for the simulations denote the standard deviation of block averages, and error bars of Kramers' theory are estimated from the dominant errors in the harmonic fits to the potentials, as shown in SI section VIII. (C) Dissociation profiles $\tau_{MFP}(x_f)$ for two methane molecules in water starting from the CP state from MD (blue solid line), from simulation of the GLE eq 1 (blue short-dashed line), from the overdamped Markovian theory eq 6 (blue long-dashed line), and from simulation of the LE eq 3 in the zero-mass limit (blue dotted line). The potential $U(x)$ is shown as a gray solid line (right scale), vertical lines denote the CP, TS, and SSP states.

the original memory time $\alpha = 1$, can be intuitively understood by a simplified picture: Memory friction pushes against the direction of the previous velocity and thereby supports barrier crossing for a certain time after an unsuccessful barrier-crossing attempt.[22] In the Markov limit $\alpha \to 0$, the GLE data converge to the result obtained by simulations of the LE with finite mass eq 3 (dash-double-dotted horizontal line), as expected. The Kramers' prediction eq 4 (dotted horizontal line) is shifted down relativ to the LE result eq 3 due to the harmonic potential approximation, as discussed before. Except an overall shift to shorter times, GH theory eq 5 (solid line) nicely reproduces the GLE data for not too large α values and converges to the Kramers' prediction in the Markovian limit $\alpha \to 0$, which reflects that GH theory can be viewed as a correction to the Kramers' theory. In the long memory-time limit, $\alpha \to \infty$, GH theory converges to the transition-state theory time and therefore misses the quadratic scaling with the memory time indicated by the black solid line.[22,39,79] We again observe that Kramers' theory (dotted horizontal line), which neglects memory effects as well as nonharmonic potential effects, agrees better with the GLE data for original memory time, i.e., for $\alpha = 1$, than GH theory, which includes memory effects, and the LE eq 3, which includes the full potential shape.

In Figure 2G, the NaCl dissociation time, τ_{MFP}, from the CP to the SSP state, using the GLE is shown as a function of the mass scaling parameter ϵ for the original memory times, i.e., for $\alpha = 1$ (circles). The dissociation time monotonically increases with growing mass. For the original mass, $\epsilon = 1$, τ_{MFP} is considerably larger than in the overdamped limit, $\epsilon \to 0$, an effect that is underestimated by Kramers' theory (dotted line), MM theory (dash-dotted line), and to a certain degree also by GH theory (solid line). So we see that inertial effects are more important for non-Markovian than for Markovian systems. GH theory and Kramers' theory converge to transition-state theory for large mass with a characteristic $\tau_{MFP} \sim \sqrt{m}$ scaling (straight broken line), which deviates from the $\tau_{MFP} \sim m$ scaling (straight solid line) for Markovian systems in the large-mass limit, as predicted by MM theory. In the low mass limit, on the other hand, Kramers' and MM theories converge. The GLE data show a slow crossover to the $\tau_{MFP} \sim m$ scaling for large mass. Again, we see that due to error cancellation, Kramers' theory agrees almost perfectly with the GLE data for original mass ($\epsilon = 1$) but also for slightly enhanced mass, as would be relevant for heavier reactants.

The dependence of the NaCl dissociation time τ_{MFP} on mass and memory time as obtained from the GLE is illustrated in Figure 2D in a contour plot as a function of α and ϵ, where three regimes can be broadly distinguished: the memory-speed-up regime (for low mass and intermediate memory time), the inertial slow-down regime (for large mass), and the memory-slow-down regime (for long memory time). The gray square indicates $\alpha = \epsilon = 1$, i.e., the original system parameters, and the gray solid lines indicate the one-dimensional cuts shown in Figure 2E−G.

In Figure 3A, we compare the NaCl dissociation time from the CP to the TS at the barrier top for the four different relevant limiting scenarios, namely (from left to right), the case with original mass and memory, the Markovian limit with original mass, the overdamped limit (using $\epsilon = 0.01$ in the GLE) with original memory, and the overdamped Markovian limit. Note that the comparison of the various limits with the original MD simulations for the transition from the CP state to the barrier top in Figure 3A is slightly different than that for the transition from the CP to the SSP state in Figure 2E−G. The blue bars denote simulation results using the GLE, eq 1, and the LE, eq 3, with the latter being used in the limit $\alpha, \epsilon \to 0$, employing the full nonharmonic potential $U(x)$. We see that the MD and GLE results for original memory and mass agree very nicely with each other. The dissociation time in the Markovian limit with original mass is roughly doubled, and in the overdamped limit with original memory, it is roughly half, compared to the MD result (denoted by a broken horizontal line). In the overdamped Markovian limit, we see that the LE simulations (blue bar) and the exact integral formula eq 6 (gray bar) agree nicely with each other, as expected, and that their agreement with the MD result is slightly better than that for the GLE results when either the original mass or memory is used. This reflects partial error compensation of the neglect of mass and memory, as amply discussed above. Kramers' theory eq 4 (yellow bar), which in addition employs a harmonic potential-shape and high-barrier approximation, slightly lowers the dissociation time and thus further improves the agreement with the MD data, another manifestation of error cancellation

https://doi.org/10.1021/acs.jpcb.2c05923
J. Phys. Chem. B 2022, 126, 10295−10304

(note that the Kramers' formula eq 4 is divided by 2 for the comparison since the final state is the barrier top). Interestingly, the well-to-barrier-top dissociation shows reduced nonharmonic potential corrections in comparison with the well-to-well dissociation discussed in Figure 2, meaning that the Kramers' result in Figure 3A (yellow bar) agrees rather well with the prediction from the integral formula eq 6 (gray bar), as will be explained in detail further below.

To demonstrate that our findings are not specific to ion dissociation, we show in Figure 3B,C results for the dissociation dynamics of a pair of methane molecules in water at 300 K (the detailed analysis is presented in SI section IX). In Figure 3C, we show the free energy from the MD simulations (gray line) together with τ_{MFP} profiles starting from the free-energy minimum, corresponding to the CP state, for varying final position x_f. We compare results from MD simulations (blue solid line) and corresponding GLE simulations (blue short-dashed line) and find, as for NaCl, good agreement. The τ_{MFP} profiles for the overdamped Markovian limit from eq 6 (blue long-dashed line) and from simulations of the LE eq 3 in the overdamped limit (blue dotted line) agree nicely with each other and are significantly higher than the MD results. The comparison of methane dissociation times from the CP to the TS at the barrier top using different approximations in Figure 3B is similar to the NaCl results in Figure 3A and demonstrates significant and compensating memory and mass effects.

All analytical rate theories we compare with, namely MM, GH and Kramers' theory, use the harmonic approximation for the well and barrier regions of the pair potentials, which becomes accurate only in the high-barrier limit. The comparison of Kramers' theory eq 4 with eq 6 in Figure 2E demonstrates that the harmonic approximation is not very good for NaCl dissociation from well to well, and it becomes better for the NaCl dissociation from well to barrier top in Figure 3A. To shed light on that, in Figure 4, we compare the τ_{MFP} from Kramers' theory eq 4 in the high-friction limit (colored solid lines) with the exact integral formula eq 6 (gray solid lines) as a function of barrier height U_0, using the potential $U(x)$ with a linearly scaled amplitude and the friction coefficient γ for NaCl from MD simulations. Data are shown for going from the CP to the TS, i.e., to the barrier top (blue and thin gray lines), and from the CP to the SSP, i.e., over the barrier from well to well (yellow and thick gray lines). The exponential scaling for $U_0 \to \infty$ is clearly seen. The relative difference between the two predictions, given in the inset, decreases with U_0, as expected. The decrease however is quite slow and scales to leading order as U_0^{-1} for the CP-SSP and as $U_0^{-1/2}$ for the CP-TS transitions, which is accurately predicted by a perturbative analysis (gray lines), see SI section III for details. The effect of the harmonic approximation is considerable for the CP-SSP transition and decreases the dissociation time by about 25% for a barrier height of $U_0 \approx 5\ k_BT$, as also seen in Figure 2D. The effect of the harmonic approximation is much less drastic for the CP-TS reaction, contrary to what would be expected based on the leading-order perturbation results, which is due to a subtle compensation of cubic and quartic potential effects at the barrier top, as explained in SI section III. Therefore, while for high barriers the harmonic-potential approximation, employed in all analytical rate theories, is valid, nonharmonic potential effects are significant at moderate barrier heights as encountered for dissociation reactions in water and many other reactions in biophysical chemistry and cannot be disregarded.

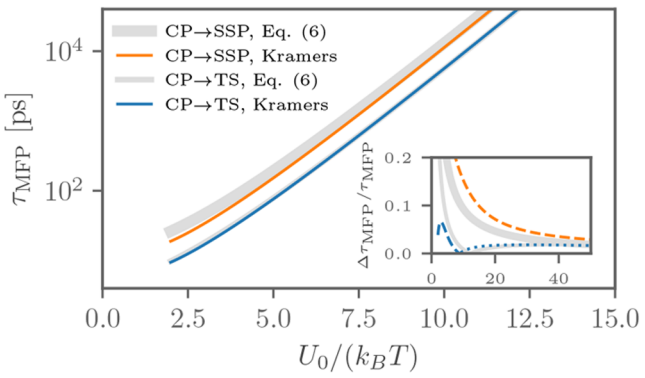

Figure 4. Effect of nonharmonic potential contributions on the NaCl dissociation dynamics in the overdamped Markovian limit. We compare τ_{MFP} given by Kramers' theory eq 4 in the high-friction limit (colored solid lines) with the integral formula eq 6 (gray solid lines) for dissociation from the CP to the TS state (blue and thin gray lines) and from the CP to the SSP state (yellow and thick gray lines) as a function of barrier height U_0. In the inset, the relative difference between the two predictions is shown as blue and yellow broken lines (dotted lines denote negative values) and compared with the perturbation prediction (gray lines); see main text for details.

CONCLUSIONS

The dissociation dynamics of a NaCl and a methane−methane pair from MD simulations is accurately reproduced using the GLE when mass, memory function and pair potential are used as extracted from MD simulations. This is a nontrivial test of the accuracy of the approximate linear friction GLE, the friction-kernel extraction techniques, and the GLE simulation methods employed by us and allows us to use the GLE as a diagnostic tool to quantitatively study how friction memory and inertial effects influence reaction kinetics. By varying the mass and the memory times in the GLE, which is not possible within MD simulations, the impact of these fundamental system properties on the reaction dynamics is quantified. It turns out that mass, memory as well as nonharmonic potential effects are important for the quantitative prediction of reaction rates of NaCl and methane in water. Due to error cancellation, Kramers' theory, that neglects memory as well as nonharmonic potential effects, performs better than GH theory, that neglects nonharmonic potential effects but approximately accounts for mass and memory effects. This in particular means that good comparison of Kramers' theory with experimental or simulated reaction times does not mean that memory effects are negligible. Our results are obtained for specific pair reactions in water, but our conclusions presumably are valid for a much wider class of systems because the GLE employed by us makes no reference to system specificities except for the mass, the memory function and the free-energy profile.

As we show in this paper, neglecting mass or memory changes the dissociation time of NaCl roughly by a factor of 2, an equivalent change of reaction time is obtained when shifting the free-energy barrier by $k_BT \ln 2 \approx 0.7\ k_BT$. So the effects we are discussing are in some sense comparable to typical experimental or theoretical uncertainties in the free-energy barriers. Nevertheless, for the quantitative prediction of reaction times and the thorough understanding of the

https://doi.org/10.1021/acs.jpcb.2c05923
J. Phys. Chem. B 2022, 126, 10295−10304

mechanisms controlling reaction times in complex systems, it is important to know how memory, mass and potential-shape effects modify reaction rates.

We extract all GLE parameters from force-field MD simulations. In the future it would be interesting to use ab initio simulations instead[80,81] and to investigate in more detail the role of the water model[81,82] for ion pair-reaction dynamics in water.

METHODS

MD simulations are performed in explicit water at 300 K, using GROMACS version 2020.6,[83] the SPC/E water force field,[84] force-field parameters for the NaCl ion pair as reported previously,[85] which are similar to recently optimized values,[86] and Lennard-Jones parameters for the methane beads from the GROMOS 53A6 force field.[87] A weak confinement potential along the connecting vector of the reactants is applied, $U_{con}(x) = kx^2/2$, with k = 100 kJ mol^{-1} nm^{-2} for NaCl and k = 30 kJ mol^{-1} nm^{-2} for methane. The cubic simulation box with side length 4 nm is completely filled with water molecules and periodic boundary conditions are applied. Before production the systems are equilibrated under NPT conditions with atmospheric pressure for 400 ps using a Berendsen barostat with a time constant of 0.5 ps and subsequently under NVT conditions for 1 ns. Production runs are performed for 200 ns under NVT conditions using the velocity rescaling thermostat with a time constant of 0.5 ps only acting on water. The simulation time step is 2 fs and correlation functions are extracted at full time resolution. The center-of-mass motion of the entire system is removed at each simulation time step. The memory kernel is extracted from correlation functions as detailed previously.[23,31] The potential, $U(x) = -k_B T \log(p(x))$, is calculated directly from the distribution function $p(x)$ with a bin size of 0.0025 nm for the ion and 0.005 nm for the methane pair.

Simulations of the GLE eq 1 using parametrized memory kernels with a sum of n exponential and l oscillating components, as given in eq 2, are performed by Markovian embedding using a fourth-order Runge–Kutta scheme.[51] The integration time step is 2 fs, equivalent to the MD simulation. When changing the mass and memory times, in particular for $\alpha, \epsilon < 1$, the simulation time step is suitably adapted. Errors of τ_{MFP}, estimated from block averages, are smaller than the symbol size. The memoryless LE eq 3 is also simulated using a fourth-order Runge–Kutta scheme. Further details on the simulation techniques is given in SI section X.

ASSOCIATED CONTENT

Data Availability Statement

The custom computer codes and input files for the simulations are available from the corresponding author upon request.

Supporting Information

The Supporting Information is available free of charge at https://pubs.acs.org/doi/10.1021/acs.jpcb.2c05923.

Detailed derivations, analysis procedures, additional data and discussion (PDF)

AUTHOR INFORMATION

Corresponding Author

Roland R. Netz – *Fachbereich Physik, Freie Universität Berlin, 14195 Berlin, Germany;* orcid.org/0000-0003-0147-0162; Email: rnetz@physik.fu-berlin.de

Authors

Florian N. Brünig – *Fachbereich Physik, Freie Universität Berlin, 14195 Berlin, Germany;* orcid.org/0000-0001-8583-6488

Jan O. Daldrop – *Fachbereich Physik, Freie Universität Berlin, 14195 Berlin, Germany*

Complete contact information is available at: https://pubs.acs.org/10.1021/acs.jpcb.2c05923

Notes

The authors declare no competing financial interest.

Biographies

Florian Brünig studied physics at the Freie Universität Berlin, Germany, where he is currently pursuing a Ph.D. degree with Prof. Roland Netz. His research interests are vibrational spectroscopy, proton dynamics, and modeling of non-Markovian effects using the generalized Langevin equation, atomistic and quantum simulations, as well as theoretical calculations.

Roland Netz studied physics at the Technical University of Berlin and at MIT and received his Ph.D. in 1994 from the University of Cologne. After postdoctoral positions at Tel-Aviv University, UC Santa Barbara, Seattle, Institute Charles Sadron in Strasbourg, CEA in Paris, and the Max-Planck Institute for Colloids and Interfaces in Potsdam, he was appointed associate professor of physics at the LMU Munich in 2002 and full professor of physics at the TU Munich in 2004. Since 2011 he has held a chair in theoretical biosoft-matter physics at the Freie Universität Berlin. His research focuses on the structure, dynamics and spectroscopy of water, proteins, polymers and charged systems using quantum, atomistic, and coarse-grained simulations as well as theoretical approaches.

■ ACKNOWLEDGMENTS

We gratefully acknowledge support by the Deutsche Forschungsgemeinschaft (DFG) Grants SFB 1078 project ID 221545957 and SFB 1114 project ID 235221301, the European Research Council (ERC) Advanced Grant NoMa-Memo Grant No. 835117, and computing time on the HPC clusters at ZEDAT and at the physics department, FU Berlin.

■ REFERENCES

(1) Kramers, H. A. Brownian motion in a field of force and the diffusion model of chemical reactions. *Physica* **1940**, *7*, 284−304.
(2) Visscher, P. B. Escape rate for a Brownian particle in a potential Well. *Phys. Rev. B* **1976**, *13*, 3272−3275.
(3) Chandler, D. Statistical mechanics of isomerization dynamics in liquids and the transition state approximation. *J. Chem. Phys.* **1978**, *68*, 2959.
(4) Skinner, J. L.; Wolynes, P. G. Relaxation processes and chemical kinetics. *J. Chem. Phys.* **1978**, *69*, 2143−2150.
(5) Arrhenius, S. Über die Reaktionsgeschwindigkeit bei des Inversion von Rohrzucker durch Säuren. *Zeit. Phys. Chem.* **1889**, *4*, 226−248.
(6) Allen, M. P. Brownian dynamics simulation of a chemical reaction in solution. *Mol. Phys.* **1980**, *40*, 1073−1087.
(7) Trullàs, J.; Giró, A.; Padró, J. A. Langevin dynamics study of NaCl electrolyte solutions at different concentrations. *J. Chem. Phys.* **1990**, *93*, 5177−5181.
(8) Lickert, B.; Stock, G. Modeling non-Markovian data using Markov state and Langevin models. *J. Chem. Phys.* **2020**, *153*, 244112.
(9) Best, R. B.; Hummer, G. Diffusive Model of Protein Folding Dynamics with Kramers Turnover in Rate. *Phys. Rev. Lett.* **2006**, *96*, 228104.
(10) Straub, J. E.; Borkovec, M.; Berne, B. J. Calculation of dynamic friction on intramolecular degrees of freedom. *J. Phys. Chem.* **1987**, *91*, 4995−4998.
(11) Hänggi, P.; Talkner, P.; Borkovec, M. Reaction-rate theory: Fifty years after Kramers. *Rev. Mod. Phys.* **1990**, *62*, 251−341.
(12) Geissler, P. L.; Dellago, C.; Chandler, D. Kinetic pathways of ion pair dissociation in water. *J. Phys. Chem. B* **1999**, *103*, 3706−3710.
(13) Mullen, R. G.; Shea, J.-E. E.; Peters, B. Transmission coefficients, committors, and solvent coordinates in ion-pair dissociation. *J. Chem. Theory Comput.* **2014**, *10*, 659−667.
(14) Roy, S.; Baer, M. D.; Mundy, C. J.; Schenter, G. K. Reaction Rate Theory in Coordination Number Space: An Application to Ion Solvation. *J. Phys. Chem. C* **2016**, *120*, 7597−7605.
(15) Takayanagi, T.; Nakatomi, T.; Yonetani, Y. On the ion-pair dissociation mechanisms in the small $NaCl\cdot(H_2O)_6$ cluster: A perspective from reaction path search calculations. *J. Comput. Chem.* **2018**, *39*, 1835−1842.
(16) Zwanzig, R. Ensemble Method in the Theory of Irreversibility. *J. Chem. Phys.* **1960**, *33*, 1338−1341.
(17) Mori, H. Transport, collective motion, and Brownian motion. *Prog. Theor. Phys.* **1965**, *33*, 423−455.
(18) Adelman, S. A. Generalized Langevin theory for many-body problems in chemical dynamics: Reactions in liquids. *J. Chem. Phys.* **1980**, *73*, 3145−3158.
(19) Ciccotti, G.; Ryckaert, J. P. On the derivation of the generalized Langevin equation for interacting Brownian particles. *J. Stat. Phys.* **1981**, *26*, 73−82.
(20) Guàrdia, E.; Padró, J. A. Generalized Langevin dynamics simulation of interacting particles. *J. Chem. Phys.* **1985**, *83*, 1917−1920.
(21) Canales, M.; Sesé, G. Generalized Langevin dynamics simulations of NaCl electrolyte solutions. *J. Chem. Phys.* **1998**, *109*, 6004−6011.
(22) Kappler, J.; Daldrop, J. O.; Brünig, F. N.; Boehle, M. D.; Netz, R. R. Memory-induced acceleration and slowdown of barrier crossing. *J. Chem. Phys.* **2018**, *148*, 014903.
(23) Daldrop, J. O.; Kappler, J.; Brünig, F. N.; Netz, R. R. Butane dihedral angle dynamics in water is dominated by internal friction. *Proc. Natl. Acad. Sci. U. S. A.* **2018**, *115*, 5169−5174.
(24) Satija, R.; Makarov, D. E. Generalized Langevin Equation as a Model for Barrier Crossing Dynamics in Biomolecular Folding. *J. Phys. Chem. B* **2019**, *123*, 802−810.
(25) Wolf, S.; Lickert, B.; Bray, S.; Stock, G. Multisecond ligand dissociation dynamics from atomistic simulations. *Nat. Commun.* **2020**, *11*, 2918.
(26) Seyler, S. L.; Pressé, S. Surmounting potential barriers: Hydrodynamic memory hedges against thermal fluctuations in particle transport. *J. Chem. Phys.* **2020**, *153*, 041102.
(27) Singh, V.; Biswas, P. A generalized Langevin equation approach for barrier crossing dynamics in conformational transitions of proteins. *J. Stat. Mech. Theory Exp.* **2021**, *2021*, 063502.
(28) Cherayil, B. J. Particle dynamics in viscoelastic media: Effects of non-thermal white noise on barrier crossing rates. *J. Chem. Phys.* **2021**, *155*, 244903.
(29) Ferrer, B. R.; Gomez-Solano, J. R.; Arzola, A. V. Fluid Viscoelasticity Triggers Fast Transitions of a Brownian Particle in a Double Well Optical Potential. *Phys. Rev. Lett.* **2021**, *126*, 108001.
(30) Meyer, H.; Wolf, S.; Stock, G.; Schilling, T. A Numerical Procedure to Evaluate Memory Effects in Non-Equilibrium Coarse-Grained Models. *Adv. Theory Simulations* **2021**, *4*, 2000197.
(31) Ayaz, C.; Tepper, L.; Brünig, F. N.; Kappler, J.; Daldrop, J. O.; Netz, R. R. Non-Markovian modeling of protein folding. *Proc. Natl. Acad. Sci. U. S. A.* **2021**, *118*, No. e2023856118.
(32) Acharya, S.; Bagchi, B. Non-Markovian rate theory on a multidimensional reaction surface: Complex interplay between enhanced configuration space and memory. *J. Chem. Phys.* **2022**, *156*, 134101.
(33) Mukherjee, S.; Mondal, S.; Acharya, S.; Bagchi, B. Tug-of-War between Internal and External Frictions and Viscosity Dependence of Rate in Biological Reactions. *Phys. Rev. Lett.* **2022**, *128*, 108101.
(34) Cherayil, B. J. Effects of Hydrodynamic Backflow on the Transmission Coefficient of a Barrier-Crossing Brownian Particle. *J. Phys. Chem. B* **2022**, *126*, 5629−5636.
(35) Satija, R.; Das, A.; Makarov, D. E. Transition path times reveal memory effects and anomalous diffusion in the dynamics of protein folding. *J. Chem. Phys.* **2017**, *147*, 152707.
(36) Carlon, E.; Orland, H.; Sakaue, T.; Vanderzande, C. Effect of Memory and Active Forces on Transition Path Time Distributions. *J. Phys. Chem. B* **2018**, *122*, 11186−11194.
(37) Singh, D.; Mondal, K.; Chaudhury, S. Effect of Memory and Inertial Contribution on Transition-Time Distributions: Theory and Simulations. *J. Phys. Chem. B* **2021**, *125*, 4536−4545.
(38) Grote, R. F.; Hynes, J. T. The stable states picture of chemical reactions. II. Rate constants for condensed and gas phase reaction models. *J. Chem. Phys.* **1980**, *73*, 2715−2732.
(39) Pollak, E.; Grabert, H.; Hänggi, P. Theory of activated rate processes for arbitrary frequency dependent friction: solution of the turnover problem. *J. Chem. Phys.* **1989**, *91*, 4073−4087.
(40) Fricks, J.; Yao, L.; Elston, T. C.; Forest, M. G. Time-Domain Methods for Diffusive Transport in Soft Matter. *SIAM J. Appl. Math.* **2009**, *69*, 1277−1308.
(41) Lei, H.; Baker, N. A.; Li, X. Data-driven parameterization of the generalized Langevin equation. *Proc. Natl. Acad. Sci. U. S. A.* **2016**, *113*, 14183−14188.
(42) Jung, G.; Hanke, M.; Schmid, F. Iterative Reconstruction of Memory Kernels. *J. Chem. Theory Comput.* **2017**, *13*, 2481−2488.
(43) Grogan, F.; Lei, H.; Li, X.; Baker, N. A. Data-driven molecular modeling with the generalized Langevin equation. *J. Comput. Phys.* **2020**, *418*, 109633.
(44) Vroylandt, H.; Goudenège, L.; Monmarché, P.; Pietrucci, F.; Rotenberg, B. Likelihood-based non-Markovian models from molecular dynamics. *Proc. Natl. Acad. Sci. U. S. A.* **2022**, *119*, No. e2117586119.

https://doi.org/10.1021/acs.jpcb.2c05923
J. Phys. Chem. B 2022, 126, 10295−10304

(45) Vroylandt, H.; Monmarché, P. Position-dependent memory kernel in generalized Langevin equations: Theory and numerical estimation. *J. Chem. Phys.* **2022**, *156*, 244105.
(46) Ciccotti, G.; Ferrario, M.; Hynes, J. T.; Kapral, R. Dynamics of ion pair interconversion in a polar solvent. *J. Chem. Phys.* **1990**, *93*, 7137−7147.
(47) Benjamin, I.; Lee, L. L.; Li, Y. S.; Liu, A.; Wilson, K. R. Generalized Langevin model for molecular dynamics of an activated reaction in solution. *Chem. Phys.* **1991**, *152*, 1−12.
(48) Rey, R.; Guàrdia, E.; Padró, J. A. Generalized Langevin dynamics simulation of activated processes in solution: Ion pair interconversion in water. *J. Chem. Phys.* **1992**, *97*, 8276−8284.
(49) Annapureddy, H. V. R.; Dang, L. X. Understanding the Rates and Molecular Mechanism of Water-Exchange around Aqueous Ions Using Molecular Simulations. *J. Phys. Chem. B* **2014**, *118*, 8917−8927.
(50) Klippenstein, V.; Tripathy, M.; Jung, G.; Schmid, F.; Van Der Vegt, N. F. Introducing Memory in Coarse-Grained Molecular Simulations. *J. Phys. Chem. B* **2021**, *125*, 4931−4954.
(51) Brünig, F. N.; Geburtig, O.; von Canal, A.; Kappler, J.; Netz, R. R. Time-Dependent Friction Effects on Vibrational Infrared Frequencies and Line Shapes of Liquid Water. *J. Phys. Chem. B* **2022**, *126*, 1579−1589.
(52) Ayaz, C.; Scalfi, L.; Dalton, B. A.; Netz, R. R. Generalized Langevin equation with a nonlinear potential of mean force and nonlinear memory friction from a hybrid projection scheme. *Phys. Rev. E* **2022**, *105*, 054138.
(53) Sedlmeier, F.; Netz, R. R. Solvation thermodynamics and heat capacity of polar and charged solutes in water. *J. Chem. Phys.* **2013**, *138*, 115101.
(54) Van Der Vegt, N. F.; Haldrup, K.; Roke, S.; Zheng, J.; Lund, M.; Bakker, H. J. Water-Mediated Ion Pairing: Occurrence and Relevance. *Chem. Rev.* **2016**, *116*, 7626−7641.
(55) Schwierz, N. Kinetic pathways of water exchange in the first hydration shell of magnesium. *J. Chem. Phys.* **2020**, *152*, 224106.
(56) Lum, K.; Chandler, D.; Weeks, J. D. Hydrophobicity at Small and Large Length Scales. *J. Phys. Chem. B* **1999**, *103*, 4570−4577.
(57) Ashbaugh, H. S.; Pratt, L. R. Colloquium: Scaled particle theory and the length scales of hydrophobicity. *Rev. Mod. Phys.* **2006**, *78*, 159−178.
(58) Sedlmeier, F.; Netz, R. R. The spontaneous curvature of the water-hydrophobe interface. *J. Chem. Phys.* **2012**, *137*, 135102.
(59) Ohtaki, H.; Radnai, T. Structure and dynamics of hydrated ions. *Chem. Rev.* **1993**, *93*, 1157−1204.
(60) Karim, O. A.; McCammon, J. A. Dynamics of a Sodium Chloride Ion Pair in Water. *J. Am. Chem. Soc.* **1986**, *108*, 1762−1766.
(61) Rey, R.; Guardia, E. Dynamical Aspects of the Na^{+}-Cl^{-} Ion Pair Association in Water. *J. Phys. Chem.* **1992**, *96*, 4712−4718.
(62) Ballard, A. J.; Dellago, C. Toward the Mechanism of Ionic Dissociation in Water. *J. Phys. Chem. B* **2012**, *116*, 13490.
(63) Wolf, S.; Stock, G. Targeted Molecular Dynamics Calculations of Free Energy Profiles Using a Nonequilibrium Friction Correction. *J. Chem. Theory Comput.* **2018**, *14*, 6175−6182.
(64) Post, M.; Wolf, S.; Stock, G. Molecular Origin of Driving-Dependent Friction in Fluids. *J. Chem. Theory Comput.* **2022**, *18*, 2816−2825.
(65) Roy, S.; Baer, M. D.; Mundy, C. J.; Schenter, G. K. Marcus Theory of Ion-Pairing. *J. Chem. Theory Comput.* **2017**, *13*, 3470−3477.
(66) Brünig, F. N.; Netz, R. R.; Kappler, J. Barrier-crossing times for different non-Markovian friction in well and barrier: A numerical study. *Phys. Rev. E* **2022**, *106*, 44133.
(67) Dalton, B. A.; Ayaz, C.; Tepper, L.; Netz, R. R.Fast protein folding is governed by memory-dependent friction. *arXiv***2022**; https://arxiv.org/abs/2208.13842.
(68) Daldrop, J. O.; Kowalik, B. G.; Netz, R. R. External Potential Modifies Friction of Molecular Solutes in Water. *Phys. Rev. X* **2017**, *7*, 041065.
(69) Marchesoni, F.; Grigolini, P. On the extension of the Kramers theory of chemical relaxation to the case of nonwhite noise. *J. Chem. Phys.* **1983**, *78*, 6287−6298.
(70) Morrone, J. A.; Markland, T. E.; Ceriotti, M.; Berne, B. J. Efficient multiple time scale molecular dynamics: Using colored noise thermostats to stabilize resonances. *J. Chem. Phys.* **2011**, *134*, 014103.
(71) Lee, H. S.; Ahn, S. H.; Darve, E. F. The multi-dimensional generalized Langevin equation for conformational motion of proteins. *J. Chem. Phys.* **2019**, *150*, 174113.
(72) Risken, H.*The Fokker−Planck Equation*, 2nd ed.; Springer: Berlin, 1996.
(73) Eyring, H. The Activated Complex in Chemical Reactions. *J. Chem. Phys.* **1935**, *3*, 107−115.
(74) Mel'nikov, V. I.; Meshkov, S. V. Theory of activated rate processes: Exact solution of the Kramers problem. *J. Chem. Phys.* **1986**, *85*, 1018−1027.
(75) Weiss, G. H. First Passage Time Problems in Chemical Physics. *Adv. Chem. Phys.* **1967**, *13*, 1−18.
(76) Hinczewski, M.; von Hansen, Y.; Dzubiella, J.; Netz, R. R. How the diffusivity profile reduces the arbitrariness of protein folding free energies. *J. Chem. Phys.* **2010**, *132*, 245103.
(77) Von Hansen, Y.; Sedlmeier, F.; Hinczewski, M.; Netz, R. R. Friction contribution to water-bond breakage kinetics. *Phys. Rev. E - Stat. Nonlinear, Soft Matter Phys.* **2011**, *84*, 051501.
(78) Kowalik, B.; Daldrop, J. O.; Kappler, J.; Schulz, J. C.; Schlaich, A.; Netz, R. R. Memory-kernel extraction for different molecular solutes in solvents of varying viscosity in confinement. *Phys. Rev. E* **2019**, *100*, 012126.
(79) Kappler, J.; Hinrichsen, V. B.; Netz, R. R. Non-Markovian barrier crossing with two-time-scale memory is dominated by the faster memory component. *Eur. Phys. J. E* **2019**, *42*, 119.
(80) Timko, J.; Bucher, D.; Kuyucak, S. Dissociation of NaCl in water from ab initio molecular dynamics simulations. *J. Chem. Phys.* **2010**, *132*, 114510.
(81) Zhang, C.; Giberti, F.; Sevgen, E.; de Pablo, J. J.; Gygi, F.; Galli, G. Dissociation of salts in water under pressure. *Nat. Commun.* **2020**, *11*, 3037.
(82) Wills, A.; Fernández-Serra, M. Role of water model on ion dissociation at ambient conditions. *J. Chem. Phys.* **2021**, *154*, 194502.
(83) Abraham, M. J.; Murtola, T.; Schulz, R.; Páll, S.; Smith, J. C.; Hess, B.; Lindahl, E. GROMACS: High performance molecular simulations through multi-level parallelism from laptops to supercomputers. *SoftwareX* **2015**, *1−2*, 19−25.
(84) Berendsen, H. J. C.; Grigera, J. R.; Straatsma, T. P. The missing term in effective pair potentials. *J. Phys. Chem.* **1987**, *91*, 6269−6271.
(85) Dang, L. X. Mechanism and Thermodynamics of Ion Selectivity in Aqueous Solutions of 18-Crown-6 Ether: A Molecular Dynamics Study. *J. Am. Chem. Soc.* **1995**, *117*, 6954−6960.
(86) Loche, P.; Steinbrunner, P.; Friedowitz, S.; Netz, R. R.; Bonthuis, D. J. Transferable Ion Force Fields in Water from a Simultaneous Optimization of Ion Solvation and Ion-Ion Interaction. *J. Phys. Chem. B* **2021**, *125*, 8581−8587.
(87) Oostenbrink, C.; Villa, A.; Mark, A. E.; Van Gunsteren, W. F. A biomolecular force field based on the free enthalpy of hydration and solvation: The GROMOS force-field parameter sets 53A5 and 53A6. *J. Comput. Chem.* **2004**, *25*, 1656−1676.

https://doi.org/10.1021/acs.jpcb.2c05923
J. Phys. Chem. B 2022, 126, 10295−10304